Theoretical Study of the O_2 Interaction with a Tetrahedral Al_4 Cluster

N. C. Bacalis,*,† A. Metropoulos,† and A. Gross‡

Theoretical and Physical Chemistry Institute, National Hellenic Research Foundation, Athens GR-11635, Greece, and Institute of Theoretical Chemistry, Ulm University, D-89069 Ulm, Germany

Received: June 7, 2010; Revised Manuscript Received: August 6, 2010

Employing both multireference configuration interaction (MRCI) and density functional theory (DFT) methods, we have studied the interaction of O_2 with a tetrahedral Al_4 cluster in the total spin triplet state. For a parallel to the base approach of O_2 facing an apex of the pyramid, the O_2 adsorption is hindered by a barrier. Both the MRCI and the DFT calculations show that after a small barrier, there are two local energy minima: a shallow one just above the apex atom and another deeper one below the apex atom. The latter corresponds to dissociative O_2 adsorption. We discuss the implications of these findings for the understanding of O_2 adsorption on defect sites of Al surfaces.

I. Introduction

The dissociative adsorption of oxygen on metal particles and surfaces is very important for heterogeneous catalysis and material processing, both of tremendous technological importance. However, whereas for the interaction of O_2 with transition metal surfaces, the microscopic reaction mechanism seems to be fairly well understood,[1−3] for the seemingly simpler system O_2/Al(111), there are still some open questions left.[4−19] Concerning the dissociative adsorption of O_2 on Al(111), molecular beam results indicate some adsorption hindrance attributed to a small barrier.[4,5]

There have been various attempts to theoretically describe this hindrance because standard electronically adiabatic periodic DFT calculation found that the dissociation of O_2 on Al(111) is not hindered by any barrier; that is, the adsorption should occur spontaneously,[8−11] in contrast to the experiment. Recently, it was shown that the low sticking probability for thermal O_2 molecules impinging on Al(111) could be explained by assuming diabatic approach of O_2 in its gas-phase triplet state without adiabatically switching to a singlet state near the surface.[12−16] This explanation has been supported by the observation of spin-selection rules in the interaction of O_2 with small Al anion clusters (∼10−20 atoms), leading to an odd/even pattern in the reactivity with O_2 as a function of the number of atoms, n, in the Al clusters.[17]

On the other hand, there have also been several other calculations, independently motivated, that provide some information about the behavior of the local environment of aluminum atoms on various adsorbents. For example, O_2 around an Al_6 cluster seems to interact somehow with apex Al atoms before eventual adsorption on the cluster;[20] also, structural deformation of surface aluminum atoms on alumina clusters causes a steric hindrance in the adsorption of NH_3 molecule.[21] These direct us to examine the possibility of steric hindrance in the adsorption of O_2 on the Al(111) surface.

In a recent paper,[18] the reactivity of O_2 ($^3\Sigma_g^-$) with planar Al_4 $^1A_1$ clusters was investigated at both the multireference configuration interaction (MRCI) and the density functional theory (DFT) levels. The motivation for that study was the question about the existence of an activation barrier in the adsorption of O_2 on an Al crystal. A comparison of the results of these two methods can be accomplished only in systems of small Al clusters in which the MRCI calculations can be applied. The MRCI calculations[18] on the interaction of O_2 with a small Al_4 cluster did yield a barrier of ∼13 kcal/mol for the square cluster geometry $^3A_1$ and about 6 kcal/mol for the rhombus geometry $^3A_2$, with the O−O axis parallel to the cluster plane. In addition, these MRCI calculations[18] indicated a dissociative adsorption when the O−O axis was vertical to the square cluster plane. Similar findings were obtained by Livshits et al.,[19] who addressed the O_2 dissociation on Al_5 clusters using hybrid DFT functionals.

The DFT results[18] showed a lack of any barrier either in the parallel or in the vertical O−O approach, which was assumed to be an artifact of the improper description of many-body effects in the employed GGA functionals. Hence, it was speculated that the absence of a minimum adsorption barrier in the periodic DFT calculations might be an artifact of the employed functionals so that there would be no need to invoke a nonadiabatic mechanism to explain the dissociative adsorption of O_2 on Al(111).

The adsorption on surfaces can be dominated by active sites that often correspond to defects;[22] however, this is not necessarily always the case, as recently shown for early transition metal surfaces.[23] To address the question whether for the O_2 adsorption on Al the considerations discussed above also apply to defect sites, in the present work, we have explored the interaction of O_2 with a small Al_4 cluster in a tetrahedral geometry, when O_2 is parallel to the pyramid basis, employing both MRCI and DFT calculations and using a richer basis set than before.[18] Thus, we also address the reliability of DFT with respect to the O_2/Al system. The calculations are not only helpful for the understanding of the interaction of O_2 with Al defect sites but should also be relevant as far as the adsorption of O_2 on small clusters is concerned.

Approaches under other angles (i.e. the largest part of phase space) are intricate and complex, involving pronounced orientational dependence, which opens up possibilities for molecular precursors and abstraction via intermediate molecularly chemisorbed states.[10] A complete study of the potential energy surface is beyond the scope of this paper (and we doubt its success

* Corresponding author. E-mail: nbacalis@eie.gr.
† National Hellenic Research Foundation.
‡ Ulm University.

10.1021/jp1052198

TABLE 1: Optimized (by analytic gradient) MRCI Energy Differences from the Ground State, And Geometries, of Al_4 Clusters in Different Structures in Their Lowest Singlet and Triplet States[a]

	ΔE (kcal/mol)	a (Å)	b (Å)	θ (deg)
square singlet	4.838	2.630	2.630	90.0
square triplet	0.226	2.684	2.684	90.0
rhombus singlet	2.636	2.603	2.603	67.7
rhombus triplet	0	2.642	2.642	75.4
rectangular singlet	8.936	2.623	2.730	90.0
rectangular triplet	2.051	2.652	2.688	90.0
tetrahedral singlet	12.776	2.683		60.0
tetrahedral triplet	9.676	2.692		60.0

[a] a and b are the side lengths in Å, and θ is the angle between the sides in degrees.

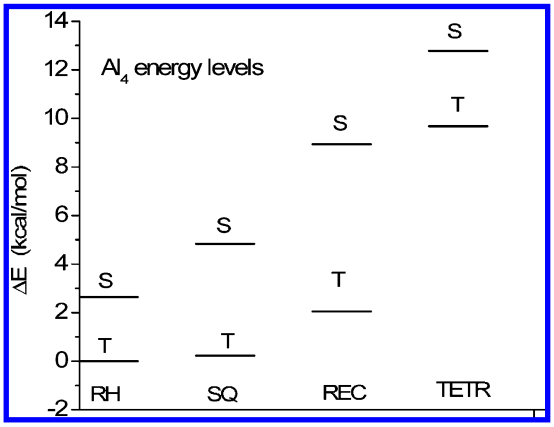

Figure 1. Total MRCI energy differences of the considered MRCI-optimized Al_4 cluster structures in the singlet (S) and triplet (T) state in kcal/mol with respect to the triplet rhombus geometry. RH, rhombus; SQ, square; REC, rectangular; TETR, tetrahedral geometries. For reference, the optimized MRCI energy of the ground state is −967.881 97 au. The optimized MRCI energies of triplet rhombus and square are rather close to each other; this, of course, does not affect the rest of present work.

because in a vertical O_2 approach, MRCI presented technical problems—e.g. convergence—and the present DFT potentials might give doubtful results).

II. Preliminary Considerations

As the first step, we address the stability, at the accurate MRCI level, of the four possible Al_4 structures that we consider here; that is, rhombus (RH), square (SQ), rectangular (REC), and tetrahedral (TETR). It is already known that the optimal geometry of the bare cluster is the planar one.[18] To simulate a defect, we set up the Al_4 cluster in a tetrahedral geometry with all sides of the pyramid of equal length so that all angles between the sides are 60°. We optimize at the MRCI level the RH, SQ, and REC geometries under pertinent constrains regarding sides and angles.

Table 1 shows the optimized MRCI geometries for each optimized structure at its lowest singlet (S) and triplet (T) states. To illustrate the energy differences between the different Al_4 structures, we plotted in Figure 1 these differences in kilocalories per mole with respect to the ground-state configuration, which is the triplet state of rhombus. The bare tetrahedral structure is shown to be ∼10 kcal/mol above the ground state of the bare rhombus. Having ascertained the energy of the optimized tetrahedral geometry relative to the planar structures, we keep this optimized geometry constant, and we use it in both the MRCI and the DFT consequent calculations. We select one apex of the pyramid as a reference point, say, Al1, and this defines a reference basis of the pyramid as the basis opposite to Al1. We take Al1 as the origin of the coordinate system with the z-axis vertical to the basis and the y-axis parallel to a side of the basis. We add an oxygen molecule above Al1 so that the O−O center of mass lies on the z-axis; its distance from the origin is denoted by ρ. The O−O line is taken to be permanently parallel to the y-axis, and the O−O distance is denoted by r.

III. Calculations

We shall see that the potential energy surface (PES) cut of this geometry shows, by both MRCI and DFT, two energy minima, a shallow one above the apex Al1, which suggests the existence of a shallow energy trap, and a deeper one below Al1. We further investigate by DFT the actual existence of an upper energy trap by relaxing all oxygen coordinates (keeping the shape and size of the pyramid fixed). Indeed, it is seen that O_2 binds slightly there, just above the apex Al1 atom, by orienting itself on a vertical mirror (σ_v) plane.

A. MRCI Calculations. For the MRCI calculations, we employed the MOLPRO package[24] with the cc-pVTZ basis set of Dunning et al.[25,26] For Al_4 in the square and rhombus geometries, the calculations were done at the D_{2h} symmetry with a self-consistent field (SCF) electron configuration of 16e on a_g, 10e on b_{3u}, 10e on b_{2u}, 6e on b_{1g}, 6e on b_{1u}, 2e on b_{2g}, and 2e on b_{3g} orbitals for the $X^3\,B_{1u}$ and $\tilde{a}^1\,A_g$ states. For a rectangle (D_{2h}), the SCF electron configurations were 12e on a_g, 4e on b_{3u}, 10e on b_{2u}, 2e on b_{1g}, 10e on b_{1u}, 2e on b_{2g}, 10e on b_{3g}, and 2e on a_u orbitals for the $X^3\,B_{1u}$ and $\tilde{a}^1\,A_g$ states. For the Al_4 cluster in tetrahedral geometry (T_d), the calculations were done at the C_s symmetry with an SCF electron configuration of 36a′/16a″ electrons for $\tilde{a}^1\,A'$ and 37a′ 15a″ electrons for $X^3\,A''$. At the multiconfiguration SCF (MCSCF) step, we employed a 12/10 reduced active space (RAS) of 12 electrons in 10 active orbitals. All the MRCI calculations were run using these reduced active space SCF (RASSCF) orbitals.

The calculations on the $Al_4 + O_2$ system were done at C_1 symmetry so that all 68 electrons were in 35 orbitals of the same symmetry with two of them singly occupied. A 20/12 RAS was adopted at the MCSCF step, in which only the four 2p electrons on each O were included in the RAS. All the MRCI calculations were run using the RASSCF orbitals.

B. DFT Calculations. The DFT calculations on the $Al_4 + O_2$ system are done at C_1 symmetry, so that all 68 electrons are in 35 Kohn−Sham orbitals of the same symmetry with the highest two of them singly occupied. We employed the Gaussian 03 package[27] using the split-valence triple-ζ basis set 6-311+g* with polarization and diffuse functions[28−30] and the Becke 3-parameter (exchange), Lee, Yang, and Parr (correlation) density functional (B3LYP).[31−34]

IV. Results and Discussion

For the MRCI calculations, we start the calculations at $\rho = 5$ Å (the distance of O_2 from the apex Al1 atom) and $r = 1.20$ Å (the internuclear O−O distance) and proceed at smaller and smaller ρ. At each ρ, only r is optimized at the CI level by running MRCI calculations at intervals of $\Delta r = 0.05$ Å. The overall system is taken to be a triplet, the same as the ground state of the gas-phase O_2.

The calculated PES cut is shown in Figure 2a, along with the curve of r, as functions of ρ. There is an activation barrier of ∼24 kcal/mol at $\rho \approx 3$ Å and a plateau at around $\rho \approx 1$ Å and $r \approx 2.7$ Å, which is the length of the pyramid side. Hence, even for the approach toward a protruding atom, the adsorption

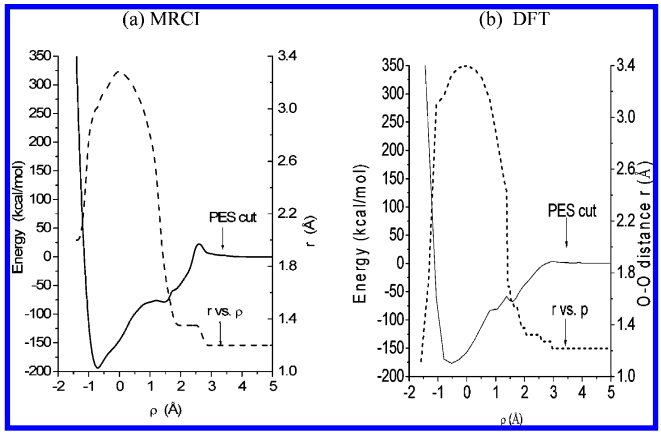

Figure 2. Graph of the PES cut of the $Al_4 + O_2$ under partial optimization of the O−O distance as O_2 attacks Al_4 along the z-axis, parallel to the pyramid basis. r is the O−O distance, and ρ is the Al_4−O_2 distance (see text). The plot of r as a function of ρ is also shown (right axis). (a) MRCI, (b) DFT results.

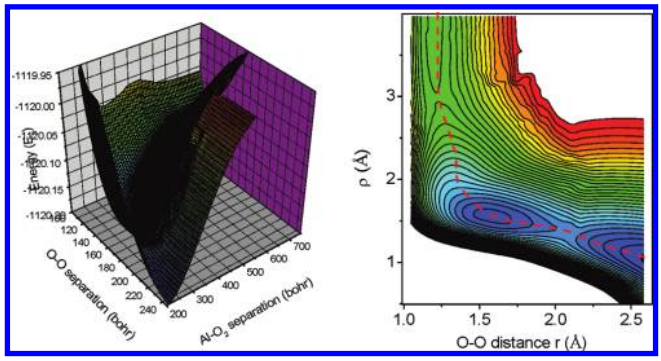

Figure 3. 3-D and contour diagram of the DFT potential energy (in a.u.) as O_2 approaches the top atom, apex of the Al_4 pyramid, for various O−O separations (in Å). The dashed line in the contour diagram, indicating the O−O bond opening, during the adsorption process, is also shown in Figure 2a and b. The energy separation of the contours is 0.01 a.u.

of O_2 on an Al cluster is activated; that is, such an adatom is not necessarily more active toward O_2 dissociation than Al atoms in a planar geometry. Since our MRCI calculations are quite accurate, we believe that the barrier at $\rho \approx 3$ Å indeed exists.

We observe that the O−O bond opens as the oxygen approaches the apex of the pyramid from 1.2 to 3.3 Å at the apex ($\rho = 0$) and then diminishes slightly to 3.0 Å at the minimum, which occurs at $\rho \approx -0.7$ Å and which is ≈200 kcal/mol lower than the asymptotic level. For $\rho < -0.7$ Å, the energy increases again, and r decreases to ∼2 Å, so it appears that in this case, O_2 forms a strong bond with Al_4, separated into two single O atoms adsorbed around the pyramid.

A completely similar picture is obtained from the DFT calculations (Figures 2b and 3a, b), which, indeed, give a slight barrier, at $\rho \approx 3$ Å, probably due to the very accurate Gaussian basis set used. This prompted us to proceed to a more extensive search of the PES using the DFT method. To investigate the plateau at around $\rho \approx 1$ Å and $r \approx 2.7$ Å, we computed the energy, E, for a systematic change of the Al−O_2 height from $\rho = -2$ to 5 Å and of the O−O separation from $r = 1$ to 5 Å, both with steps of 0.1 Å.

Figure 3 displays the DFT potential energy surface $E(r, \rho)$ around the plateau. We observe that as O_2 approaches the pyramid from above, there are, apart from the free O_2 local energy minimum at an O−O distance of $r = 1.2$ Å for an Al−O_2 separation $\rho > 3$ Å, two local energy minima. At $\rho \approx 3$ Å above

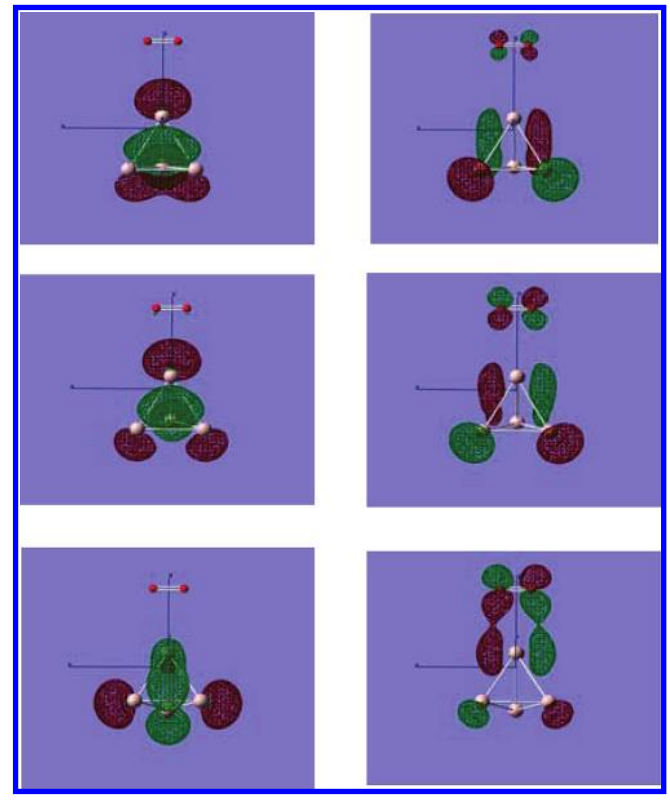

Figure 4. Isovalue plots of the spin-up (left panel) and spin-down (right panel) HOMO of the triplet state, around the first, most remote transition barrier at a distance of $\rho \approx 3$ Å from the Al1 atom, as O_2 approaches the top of the Al_4 pyramid. During the transition, O_2 attracts some electronic charge density from the cluster.

the Al1 apex, a first barrier toward O_2 adsorption occurs, although much shallower than the corresponding MRCI barrier (of ∼24 kcal/mol, which we believe) at $\rho \approx 3$ Å. (In our previous paper,[18] the DFT calculation, done with lower quality basis functions, around this area had failed.) After this barrier, there is a slight O−O bond elongation to a length of $r = 1.4$ Å. At about $\rho = 1.5$ Å, there is a local energy minimum with an O−O distance of $r = 1.6$ Å, corresponding to where there is a slight binding of each O atom with the Al cluster apex atom Al1. We will further investigate this local minimum below. Just below this local minimum, a second, more important, transition occurs, at an O−O distance of 2.1 Å, before the O atoms are finally separated toward adsorption between the surface and the apex Al1 atom of the Al_4 pyramid.

The dashed line in the contour diagram of Figure 3, indicating the O−O bond opening during the adsorption process, is also shown in Figure 2a and b. The above behavior is consistently reproduced by both employed calculational methods, MRCI and DFT, despite the fact that the DFT remote barrier at $\rho \approx 3$ Å is much shallower than that of MRCI (see also Figure 4).

To obtain an idea of the electron redistribution in passing, consecutively, through the above two transitions, we examined the corresponding Kohn−Sham highest occupied molecular orbitals (HOMO), as shown in the next figures.

Figure 4 shows the HOMO orbitals around the first (remote) transition from molecular O_2 toward the intermediate trap. The second row corresponds to the transition (on the examined plane), and the first and third rows correspond to O_2 positions just above and below the remote barrier. The spin-up HOMO (left side of Figure 4) belongs entirely to the Al pyramid, but through the spin-down HOMO (right side of Figure 4), some

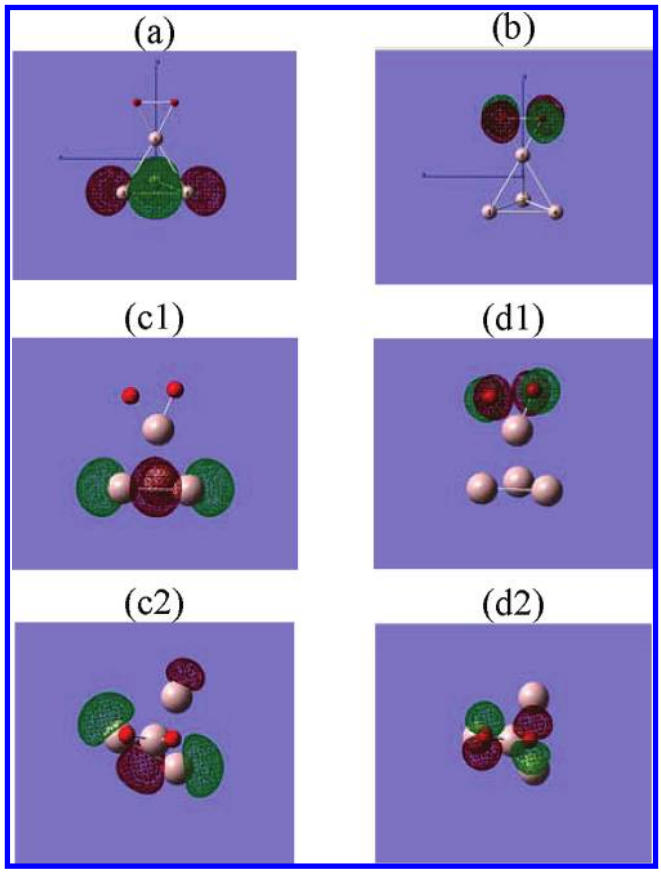

Figure 5. The triplet spin-up (left panel) and spin-down (right panel) HOMO at the local trap at $\rho \approx 1.5$ Å of Figure 3 (a, b), as well as at the optimized trap geometry (c, d). (c1, d1), side view; (c2, d2), top view.

electron density is transferred from the Al pyramid to O_2, as clearly seen at the first local minimum in Figure 5.

The first row of Figure 5 shows the HOMO orbitals (left panel, spin-up; right panel, spin-down) at the first local minimum on the plane of Figure 3 (close to the actual trap), where O_2 is still parallel to one vertex of the triangular basis. The Al1−O bond length is 1.7 Å; the O−Al1−O angle is 65°.

To investigate this trap, we relaxed the two O atoms to optimize their geometry. Indeed, as seen in the two lower rows of Figure 5, they are trapped above the Al1 apex, rotated so that one O atom stabilizes on the extension of one of the side vertices, while the other stabilizes above the same vertex. The binding energy (from the free O_2) is ∼70 (DFT value) to 80 (MRCI value) kcal/mol. At the trap, there are three kinds of eigen frequencies: two higher (963 and 787 cm^{-1}, where the two O atoms vibrate with respect to Al1 in phase and out of phase, respectively; the Al1−O bond length changes), three intermediate (340, 309, and 266 cm^{-1}, corresponding to O−Al1−O angular oscillations; the Al1−O bond length is unchanged, while the triangular Al basis oscillates slightly, too), and five lower (213, 180, 172, 148, and 51 cm^{-1}, where the $Al1O_2$ moiety moves with respect to the triangular basis as a whole). In this geometry, there are also two imaginary frequencies at which the triangular basis internally oscillates (linearly and rotationally) with respect to a fixed $Al1O_2$ moiety, indicating that this structure is not the ground state of this whole "molecule". Therefore, we checked whether this trap could still exist in a slightly more realistic Al(111) surface environment. We surrounded the triangular basis with 9 more Al atoms (all 12 forming a (111) structure) while keeping the Al1 apex above the central triangle, and we relaxed the two O atoms around the trap, thus modelling an adatom at a (111) surface. The trap still exists in such a configuration (Figure 6).

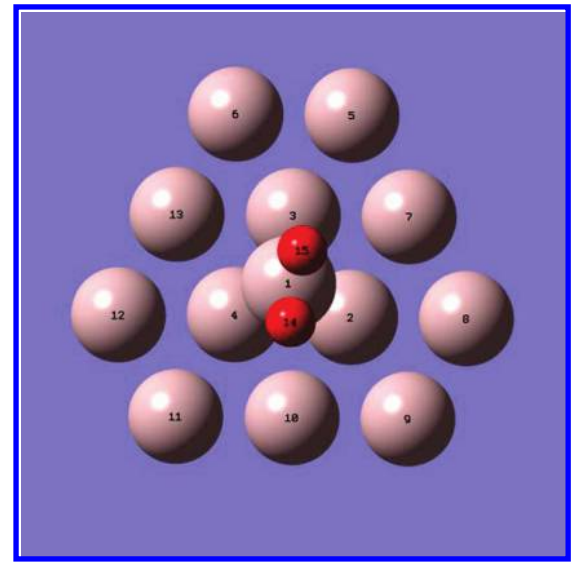

Figure 6. Structure of the O_2 molecule temporarily trapped above an apex Al atom on top of a flat Al_{12} cluster modeling an adatom at the (111) surface.

The relevant eigen frequencies in the larger cluster are in the same order of magnitude as in the tetrahedron case, that is, 700−900 cm^{-1} for the O vibrations, 250−350 cm^{-1} for the O rotational oscillations, and 50−200 cm^{-1} for the $Al1O_2$ movements. Thus, we believe that if there are apex-Al atoms above the Al (111) surface, the incoming O_2 is temporarily trapped (delayed) by them, but the time delay, ∼40 fs, is experimentally rather undetectable. In the trap, the two O atoms are negatively charged by 0.2 *e* each, (Mulliken population) taken from the triangular basis, and the apex Al1 is neutral.

Next, we were not able to find the transition state from this trap toward the lower lying adsorption state, but since there is no essential difference in the orbitals of the actual trap and of the local minimum of Figure 3, (cf. Figure 5a,b vs c,d), we show, indicatively, in Figure 7 the electron density transfer around the second (lower) barrier of Figure 3.

Figure 7 shows the spin-up and spin-down HOMO of the triplet, around the transition barrier (height of ≈1.5 Å), as O_2 approaches the top of the Al_4 pyramid. The second row corresponds to the barrier; the first and third rows correspond to O_2 positions just above and below the barrier: The spin-down HOMO changes entirely during the transition; the spin-up HOMO is affected, but eventually it remains unaltered. The barrier from the trap toward the final adsorption state is ∼10 kcal/mol, and the difference between the trap and the final adsorption state is ∼115 (DFT) to 120 (MRCI) kcal/mol.

V. Conclusions

We examined the adsorption of O_2 on an apex atom of an Al_4 tetrahedron of 2.7 Å Al−Al bond length (in the total spin triplet state) by both ab initio MRDCI and DFT methods. Such a configuration might be relevant for the understanding of the interaction of O_2 with defect sites on Al, such as adatoms. We found, similar to other DFT calculations of O_2 interacting with small flat Al clusters using hybrid functional, that the O_2 adsorption at the apex of the cluster is hindered by a barrier. This means that an Al adatom is not necessarily more active toward O_2 dissociation than Al atoms in a planar geometry. This

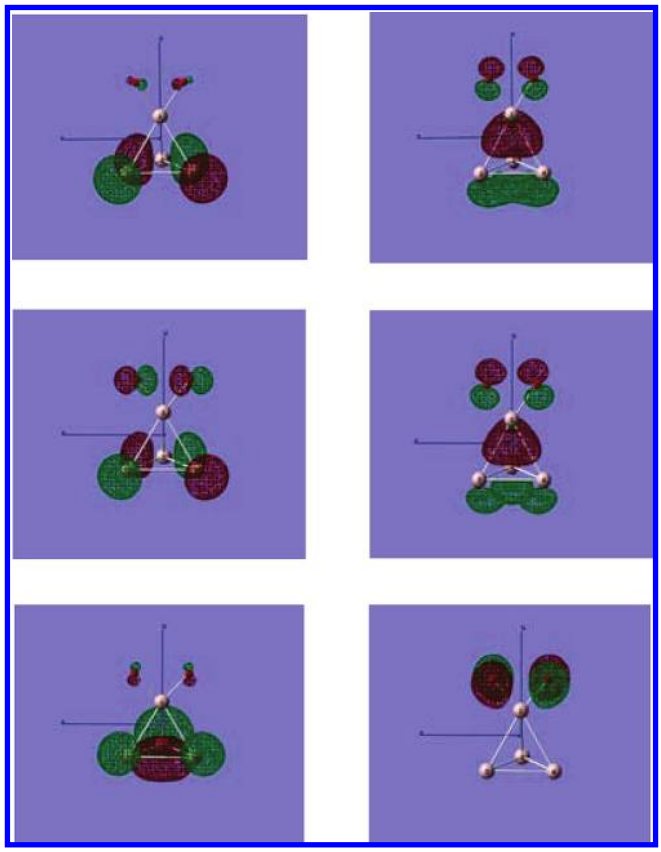

Figure 7. The spin-up and spin-down HOMO of the triplet, around the transition barrier at a distance of $\rho \approx 1.5$ Å, as O_2 approaches the top of the Al_4 pyramid, leaving the trap. The O atoms still attract some electronic charge density from the cluster.

also means that the vanishing barrier for the O_2 adsorption on Al(111) found in periodic DFT calculations might still be an artifact of the employed functionals (rather than the basis functions), as indicated by the larger barrier found in MRCI calculations than in DFT calculations.

Using DFT, we mapped out the potential energy surface of the O_2-Al_4 interaction in some more detail. According to these calculations, O_2 can be temporarily trapped to a local energy minimum above the apex while approaching the apex of the pyramid, resulting in as yet experimentally undetectable time delay of about 40 fs before it is finally adsorbed dissociatively below the apex (in a deeper energy minimum): When O_2 approaches the apex Al atom, the elongated O_2 molecule is trapped on top of it with a binding energy (relative to the free O_2) of $\sim$70−80 kcal/mol before it overcomes a barrier of $\sim$10 kcal/mol toward full dissociative adsorption below the apex Al atom, $\sim$115−120 kcal/mol lower than the trap. In the trap, O_2 attracts some electronic charge from the cluster basis Al atoms ($\approx$0.4e in Mulliken population), whereas the intermediate apex Al atom is neutral. Of course, this charge transfer refers to our small cluster with a limited number of electrons and not to a semi-infinite substrate with an infinite reservoir of electrons at the Fermi level.

Acknowledgment. This work was supported in part by the IKYDA program of the German Academic Exchange Service (DAAD) and the Greek State Scholarships Foundation (I.K.Y.). Partial support of this work through the Excellence in the Research Institutes program, supervised by the General Secretariat for Research and Technology/Ministry of Development, Greece (Phase I and II, Projects 64769 and 200501330081) is gratefully acknowledged.

References and Notes

(1) Eichler, A.; Hafner, J. *Phys. Rev. Lett.* **1997**, *79*, 4481.
(2) Gross, A.; Eichler, A.; Hafner, J.; Mehl, M. J.; Papaconstantopoulos, D. A. *Surf. Sci.* **2003**, *539*, L542.
(3) Lischka, M.; Mosch, C.; Gross, A. *Electrochim. Acta* **2007**, *52*, 2219.
(4) Brune, H.; Wintterlin, J.; Behm, R. J.; Ertl, G. *Phys. Rev. Lett.* **1992**, *68*, 624.
(5) Österlund, L.; Zorić, I.; Kasemo, B. *Phys. Rev. B* **1997**, *55*, 15452–15455.
(6) Zhukov, V.; Popova, I.; Yates, J. T. *Surf. Sci.* **1999**, *441*, 251.
(7) Binetti, M.; Weisse, O.; Hasselbrink, E.; Katz, G.; Kosloff, R.; Zeiri, Y. *Chem. Phys. Lett.* **2003**, *373*, 366.
(8) Sasaki, T.; Ohno, T. *Surf. Sci.* **1999**, *433*, 172.
(9) Honkala, K.; Laasonen, K. *Phys. Rev. Lett.* **2000**, *84*, 705.
(10) Yourdshahyan, Y. Y.; Razaznejad, B.; Lundqvist, B. I. *Phys. Rev. B* **2002**, *65*, 075416.
(11) Zhukovskii, Yu. F.; Jacobs, P. W. M.; Causá, M. *J. Phys. Chem. Sol.* **2003**, *64*, 1317.
(12) Behler, J.; Delley, B.; Lorenz, S.; Reuter, K.; Scheffler, M. *Phys. Rev. Lett.* **2005**, *94*, 036104.
(13) Behler, J.; Delley, B.; Reuter, K.; Scheffler, M. *Phys. Rev. B* **2007**, *75*, 115409.
(14) Behler, J.; Reuter, K.; Scheffler, M. *Phys. Rev. B* **2008**, *77*, 115421.
(15) Carbogno, C.; Behler, J.; Gross, A.; Reuter, K. *Phys. Rev. Lett.* **2008**, *101*, 096104.
(16) Carbogno, C.; Behler, J.; Reuter, K.; Gross, A. *Phys. Rev. B* **2010**, *81*, 035410.
(17) Burgert, R.; Schnöckel, H.; Grubisic, A.; Li, X.; Bowen, S. T. S. K. H.; Ganteför, G. F.; Kiran, B.; Jena, P. *Science* **2008**, *319*, 438.
(18) Mosch, C.; Koukounas, C.; Bacalis, N.; Metropoulos, A.; Gross, A.; Mavridis, A. *J. Phys. Chem. C* **2008**, *112*, 6924.
(19) Livshits, E.; Baer, R.; Kosloff, R. *J. Phys. Chem. A* **2009**, *113*, 7521.
(20) Hoshino, T.; Sekino, A.; Hata, M.; Tsuda, M. *Appl. Surf. Sci.* **2000**, *162*, 435.
(21) Tachikawa, H.; Tsuchida, T. *J. Mol. Catal., A* **1995**, *96*, 277.
(22) Gross, A. *J. Comput. Theor. Nanosci.* **2008**, *5*, 894.
(23) Schnur, S.; Gross, A. *Phys. Rev. B* **2010**, *81*, 033402.
(24) *MOLPRO*, a package of programs written by Werner, H. J.; Knowles, P. J. with contributions fromAlmlof, J., Amos, R. D.
(25) Dunning, T. H., Jr. *J. Chem. Phys.* **1989**, *90*, 1007.
(26) Kendall, R. A.; Dunning, T. H., Jr.; Harrison, R. J. *J. Chem. Phys.* **1992**, *96*, 6769.
(27) Frisch, M. J.; Trucks, G. W.; Schlegel, H. B.; Scuseria, G. E.; Robb, M. A.; Cheeseman, J. R.; Montgomery, J. A., Jr.; Vreven, T.; Kudin, K. N.; Burant, J. C.; Millam, J. M.; Iyengar, S. S.; Tomasi, J.; Barone, V.; Mennucci, B.; Cossi, M.; Scalmani, G.; Rega, N.; Petersson, G. A.; Nakatsuji, H.; Hada, M.; Ehara, M.; Toyota, K.; Fukuda, R.; Hasegawa, J.; Ishida, M.; Nakajima, T.; Honda, Y.; Kitao, O.; Nakai, H.; Klene, M.; Li, X.; Knox, J. E.; Hratchian, H. P.; Cross, J. B.; Adamo, C.; Jaramillo, J.; Gomperts, R.; Stratmann, R. E.; Yazyev, O.; Austin, A. J.; Cammi, R.; Pomelli, C.; Ochterski, J. W.; Ayala, P. Y.; Morokuma, K.; Voth, G. A.; Salvador, P.; Dannenberg, J. J.; Zakrzewski, V. G.; Dapprich, S.; Daniels, A. D.; Strain, M. C.; Farkas, O.; Malick, D. K.; Rabuck, A. D.; Raghavachari, K.; Foresman, J. B.; Ortiz, J. V.; Cui, Q.; Baboul, A. G.; Clifford, S.; Cioslowski, J.; Stefanov, B. B.; Liu, G.; Liashenko, A.; Piskorz, P.; Komaromi, I.; Martin, R. L.; Fox, D. J.; Keith, T.; Al-Laham, M. A.; Peng, C. Y.; Nanayakkara, A.; Challacombe, M.; Gill, P. M. W.; Johnson, B.; Chen, W.; Wong, M. W.; Gonzalez, C.; Pople, J. A. *Gaussian 03, Revision C.02*; Gaussian, Inc.: Wallingford, CT, 2004.
(28) McLean, A. D.; Chandler, G. S. *J. Chem. Phys.* **1980**, *72*, 5639.
(29) Krishnan, R.; Binkley, J. S.; Seeger, R.; Pople, J. A. *J. Chem. Phys.* **1980**, *72*, 650.
(30) Frisch, M. J.; Pople, J. A.; Binkley, J. S. *J. Chem. Phys.* **1984**, *80*, 3265.
(31) Becke, A. D. *J. Chem. Phys.* **1993**, *98*, 1372.
(32) Lee, C.; Yang, W.; Parr, R. *Phys. Rev. B* **1988**, *37*, 785.
(33) Vosko, S. H.; Wilk, L.; Nusair, M. *Can. J. Phys.* **1980**, *58*, 1200.
(34) Stephens, P. J.; Devlin, F. J.; Chabalowski, C. F.; Frisch, M. J. *J. Phys. Chem.* **1994**, *98* (45), 11623–11627.

JP1052198